

SHORT COMMUNICATION

Climatological representation of mesoscale convective systems in a dynamically downscaled climate simulation

Alex M. Haberie¹  | Walker S. Ashley² 

¹Department of Geography and Anthropology,
Louisiana State University, Baton Rouge,
Louisiana

²Department of Geographic and Atmospheric
Sciences, Northern Illinois University, DeKalb,
Louisiana

Correspondence

Alex Haberie, Department of Geography and
Anthropology, Louisiana State University, Baton
Rouge, LA 70803.

Email: ahaberlie1@lsu.edu

Funding information

Division of Atmospheric and Geospace Sciences,
Grant/Award Number: ATM-1637225

This research assesses the utility and validity of using simulated radar reflectivity to detect potential changes in linear and nonlinear mesoscale convective system (MCS) occurrence in the Midwest United States between the early and late 21st century using convection-permitting climate simulation output. These data include a control run and a pseudo-global warming (PGW) run that is based on RCP 8.5. First, using a novel segmentation, classification, and tracking procedure, MCS tracks are extracted from observed and simulated radar reflectivity. Next, a comparison between observed and the control run MCS statistics is performed, which finds a negative summertime bias that agrees with previous work. Using a convolutional neural network to perform probabilistic predictions, the MCS dataset is further stratified into highly organized, quasi-linear convective systems (QLCSs)—which can include bow echoes, squall lines, and line echo wave patterns—and generally less-organized, non-QLCS events. The morphologically stratified data reveal that the negative MCS bias in this region is largely driven by too few QLCSs. Although comparisons between the control run and a PGW run suggest that all MCS events are less common in the future (including QLCS and non-QLCS events), these changes are not spatially significant, whereas the biases between the control run and observations are spatially significant. A discussion on the importance and challenges of simulating QLCSs in convection-permitting climate model runs is provided. Finally, potential avenues of exploration are suggested related to the aforementioned issues.

KEYWORDS

climate modeling, mesoscale convective systems, convolutional neural network

1 | INTRODUCTION

The Intergovernmental Panel on Climate Change's Fifth Assessment Report (IPCC, 2013) states that heavy precipitation events are likely to increase in frequency during the 21st century. The report, however, makes broad generalizations regarding regional thunderstorm activity (Tippett *et al.*, 2015), admitting that deep moist convection (DMC) occurrence is highly variable and sensitive to remote (teleconnections) and local forcings (Diffenbaugh *et al.*, 2008; Kendon *et al.*, 2014). Compounding these issues, the report relied on coarse-resolution global circulation models (GCMs), which generally cannot resolve phenomena with important meso- γ (i.e., <10 km) features. This is particularly concerning for the central and eastern Conterminous United States (CONUS), where mesoscale convective systems (MCSs) produce a large

percentage of warm-season precipitation (Ashley *et al.*, 2003; Houze, 2004). In addition, quasi-linear MCSs (QLCSs), which include highly organized system morphologies such as bow echoes, squall lines, and line echo wave patterns, regularly produce tornadoes, hail, nontornadic damaging winds, and derechos (Trapp *et al.*, 2005), as well as extreme precipitation rates (Stevenson and Schumacher, 2014).

Previous modelling work has suggested that high-resolution (i.e., ≤ 4 km spatial and 1-hr temporal) runs of regional climate models (RCMs) are required to accurately reproduce the location, morphology, evolution, and intensity of MCSs and other DMC phenomena (Weisman *et al.*, 1997; Herman and Schumacher, 2016). This is because meso- γ processes that commonly occur within sub-hourly timescales—such as those associated with the interaction of individual DMC updraughts—are crucial to the development and

sustenance of MCSs. Thus, even relatively high-resolution GCM simulations (e.g., 10^2 km spatial and 6-hr temporal) are unable to explicitly simulate these important mechanisms (Prein *et al.*, 2015). Using GCMs or other relatively coarse-resolution model output as initial and boundary conditions to drive a RCM (dynamical downscaling; Trapp *et al.*, 2011; Gensini and Mote, 2014; Liu *et al.*, 2017) is one widely used approach used to examine DMC phenomena in the context of long-term (i.e., ≥ 10 years) climate simulations. Dynamically downscaled climate simulations have been found to reasonably reproduce observations of rainfall and convective hazards associated with DMC phenomena (Trapp *et al.*, 2011; Gensini and Mote, 2014; Liu *et al.*, 2017; Prein *et al.*, 2017a).

In the central and eastern CONUS, heavy rain events associated with DMC are becoming more frequent (Kunkel *et al.*, 2013), and climate simulations suggest that this trend should continue through the 21st century (Tippett *et al.*, 2015). This trend is cause for concern, as three of the most extreme drought and flood years in recent memory (1993, 1998, 2012) resulted in combined losses exceeding \$100 billion in the United States (Smith and Katz, 2013). These changes may be caused, in part, by the modification of MCSs in a changing climate (Feng *et al.*, 2016; Prein *et al.*, 2017b). Changes in important meteorological factors that could influence future MCSs evolution include low- and mid-level specific humidity, instability (i.e., CAPE), the frequency of the Great Plains low-level jet, and cold pool development and strength (Harding and Snyder, 2015; Feng *et al.*, 2016; Tang *et al.*, 2017; Prein *et al.*, 2017b). These factors may work in concert to generate MCSs that are larger, produce more rainfall, and exhibit faster forward propagation (Prein *et al.*, 2017b), although the spatial pattern of these changes may vary (Rasmussen *et al.*, 2017).

The purpose of this study is to address the following research questions: (a) *Can long-term climate simulations recreate an observed climatology of Midwest CONUS QLCSs?*; and if so (b) *Does Midwest CONUS QLCS occurrence change in a late-21st century climate simulation?* To answer these questions, data generated by two long-term (13 years), high-resolution (4 km) pseudo-global warming (PGW) (Ikeda *et al.*, 2010) climate simulations (Liu *et al.*, 2017) encompassing the CONUS are compared and analysed using an MCS and QLCS detection and tracking framework. Specifically, simulated composite reflectivity from both a control simulation (CTRL) and a PGW simulation are used to explicitly examine potential changes in QLCS occurrence in the central and eastern CONUS. The model data and approach are described in Section 2. The use of simulated reflectivity to identify QLCSs in climate simulation output is novel and extends recent work that identified MCSs using accumulated grid-scale precipitation (Prein *et al.*, 2017a, 2017b). To assure precision and comparability, a segmentation, classification, and tracking procedure is uniformly applied to observed (OBS), CTRL, and PGW composite reflectivity to detect QLCS and non-QLCS events (Haberlie and Ashley, 2018a, 2018b). Since QLCS produce multifaceted hazards and are an important part of the eastern CONUS hydroclimate (Houze, 2004; Harding and Snyder,

2015), these results may have far-reaching implications for many aspects of society. In addition, the event-identification machine learning technique described in this article could be modified for many different applications in climate science.

2 | DATA AND METHODOLOGY

These simulations employed original and modified ERA-interim (Dee *et al.*, 2011) data as lateral boundary conditions to drive the Weather Research and Forecasting (WRF) model. The simulation using unmodified ERA-interim data serve as an early 21st century control, with a study period from October 2000 to September 2013, inclusive. To simulate a potential late-21st century scenario, the unmodified ERA-interim data are perturbed using a PGW approach (Ikeda *et al.*, 2010). The perturbation value for each of these variables is calculated by finding the mean multimodel (cf. Table 1 in Liu *et al.*, 2017) difference between late 21st century (2071–2100) and late 20th and early 21st century (1976–2005) values derived from RCP 8.5 climate simulations (IPCC, 2013). Accumulated grid-scale precipitation and hourly simulated composite reflectivity derived from CTRL has been shown to reasonably reproduce spatial patterns of convection in the central and eastern CONUS (Rasmussen *et al.*, 2017), although rainfall exhibits an overall negative bias during meteorological summer (Liu *et al.*, 2017). For a comparative observational dataset, the National Operational Weather Radar (NOWrad™) dataset—which are national mosaics of composite reflectivity—are used to verify the occurrence of MCSs and QLCSs. These data have ~ 2 -km horizontal resolution and have been used in many radar climatology studies (Matyas, 2010; Fabry *et al.*, 2017). Previous work has also compared structures within simulated reflectivity factor and observed reflectivity data, despite the well-known biases (Lawson and Gallus, 2016; Matyas *et al.*, 2018). The study period runs from January 2000 to September 2013, with an emphasis on the months of June, July, and August from 2001 to 2013. The research focuses on the Midwest CONUS due to its high level of MCS activity (e.g., Ashley *et al.*, 2003) and this region is defined as in Prein *et al.* (2017a). To limit biases due to projection and resolution issues, NOWrad data from the top of each available hour are first interpolated to the modelled grid points (see: <https://rda.ucar.edu/datasets/ds612.0/>) using a nearest neighbour approach. All distances and areas are then calculated assuming a pixel size of 4×4 km (16 km^2).

MCSs are identified in the composite reflectivity images using a combination of image segmentation and machine learning (McGovern *et al.*, 2017) approaches (Haberlie and Ashley, 2018a, 2018b). Automated methods are used instead of subjective methods because of the large number of events ($N = 10^4$) and hourly images ($N = 10^6$) included in the study. This approach is based on the Parker and Johnson (2000) definition of MCSs—namely, that they are contiguous swaths of precipitation that last for at least 3 hr and are generated by connected or nearly connected convective updrafts. First, convective (≥ 40 dBZ) cells with intense (≥ 50 dBZ) rainfall

are identified and aggregated into regions based on a 24-km search radius. Connected regions with a major axis length exceeding 100 km are associated with stratiform (≥ 20 dBZ) precipitation regions within 96 km (slices). Using an ensemble machine learning classifier, each slice is then given a probabilistic classification of MCS (e.g., areal, leading/trailing/no stratiform, squall lines, hybrid, etc.) or non-MCS (e.g., ground clutter, tropical systems, synoptic systems, and unorganized convective clusters). MCS slices are associated spatiotemporally into MCS swaths by checking for spatiotemporal overlap (as shown in Figure S1 in Appendix S1, Supporting Information). Ties are broken by connecting the most similar slices together (Hungarian method; Munkres, 1957; Lakshmanan *et al.*, 2013). To improve the specificity of swaths (i.e., only examine swaths very likely to be MCSs), a 0.95 MCS probability (P_{MCS}) threshold is employed, and slices below this threshold are not considered in the swath-building process. Once swaths are generated, only those swaths that last at least 3 hr (Parker and Johnson, 2000) are considered MCS swaths (herein $P_{\text{MCS}95}$ swaths).

QLCSs (and non-QLCSs) are identified within the MCS dataset using an image classification algorithm that assigns a probabilistic label (herein, P_{QLCS}) ranging from 0 (very likely a non-QLCS) to 1 (very likely a QLCS). This is performed using a convolutional neural network (CNN; Krizhevsky *et al.*, 2012) with an architecture similar to a single CNN described in Dieleman *et al.* (2015) (as reported in Table S1, Supporting Information). The choice of using a CNN instead of traditional machine learning algorithms is motivated by the similarity of features extracted from the QLCS and non-QLCS samples (as shown in Figure S2 in Appendix S1), which can result in relatively poor classification performance for those types of algorithms.

To generate training and testing data, nearly 3,000 slices are randomly selected from $P_{\text{MCS}95}$ swaths generated from observed composite reflectivity data. These slices are then hand-labelled as QLCS or non-QLCS. QLCS events are subjectively identified using the following criteria: (a) convective regions within slices had to be longer than 100 km and (b) these convective regions have to be at least three times as long as they are wide (Trapp *et al.*, 2005; Gallus *et al.*, 2008). In addition, the spatial structure of slices identified as QLCS are subjectively judged as belonging to one of the following pre-existing categories: trailing stratiform, leading stratiform, or parallel stratiform (Parker and Johnson, 2000). In total, 1,087 QLCS and 1,835 non-QLCS slices are subjectively classified by the authors, and of this population, approximately 80% of the samples were used for training purposes, leaving 198 QLCS and 387 non-QLCS to assess model performance. The CNN is trained by extracting pixels from a 256×256 km region centred on the most intense portion of the slice ("storm patches"; Gagne *et al.*, 2017). Data augmentation (Krizhevsky *et al.*, 2012; Dieleman *et al.*, 2015) is performed using the training data by: (a) randomly rotating the

images by $\pm 20^\circ$ and (b) randomly scaling the width and height of the images by $\pm 20\%$. Data augmentation is used when training CNNs to prevent overfitting and improve testing performance (Krizhevsky *et al.*, 2012), essentially preventing the model from memorizing the training data (Dieleman *et al.*, 2015). For this article, the result is the orientation and size of the MCS is de-emphasized, whereas the relative spatial structure of rainfall intensity is emphasized.

The trained model correctly predicts 370 out of 387 non-QLCS slices (96%) and 172 out of 198 QLCS slices (87%). This suggests that model predictions of QLCSs may be slightly conservative, since although 9% of non-QLCS slices are labelled as QLCSs (false positives), 13% of QLCS slices are labelled as non-QLCSs (false negatives). The model produces an area under the curve of 0.98 and a brier loss score of 0.054, which is a marked improvement of false positive/false negative balance and probabilistic classification reliability over the more traditional machine learning algorithms (as shown in Figure S3 in Appendix S1). In addition, a subjective examination of events labelled with high (as shown in Figure S4 in Appendix S1) and low (as shown in Figure S5 in Appendix S1) QLCS probabilities (herein P_{QLCS}) reveals that the algorithm produces reasonable predictions. In general, samples with high P_{QLCS} (i.e., ≥ 0.95) exhibited linear structures (bow echoes, line echo wave patterns, leading line trailing stratiform, etc.), whereas samples with low P_{QLCS} (i.e., ≤ 0.05) exhibited more nonlinear MCS structures (areal, broken line, etc.). Using the predictions from this model, an MCS swath is considered a QLCS when it is assigned a P_{QLCS} greater than or equal to 0.50 for at least two consecutive hours (Gallus *et al.*, 2008). The spatial occurrence of swaths is upscaled from the 4 to 40-km grids by calculating the mean occurrence within the larger grid. In addition, 40-km grids were chosen to reduce the influence of small-scale noise in the OBS data (ground clutter, anomalous propagation, etc.), while also being comparably sized with quantitative precipitation forecast guidance grids and similar studies (e.g., Clark *et al.*, 2014; Novak *et al.*, 2014).

3 | EVENT DAY OCCURRENCE

The statistics of QLCS, non-QLCS, and combined events (i.e., MCSs) are examined for the Midwest CONUS. The following analyses report counts of MCS, QLCS, and non-QLCS days (herein, event days), which is defined as any 1800 UTC to 1800 UTC period during which an event occurred within the study area or grid cell. From October 2000 to September 2013, there were 1,800 OBS, 1,738 CTRL, and 1,850 PGW MCS event days. Approximately 49% of all OBS MCS event days occur during meteorological summer (June–August), compared to 29% in the spring (March–May), 18% in the fall (September–November), and 4% in the winter (December–February). July is the most active month for OBS MCSs, with 17% of all MCS event days occurring in this month. For QLCSs, there were 1,200 OBS, 743 CTRL, and 848 PGW event days. The frequency

of OBS QLCS event days peaks during June (19%), whereas the frequency of OBS non-QLCS event days peaks during July (19%). Similarly, the frequency of CTRL MCS, QLCS, and non-QLCS event days peaks during June (17, 25, and 18%, respectively). Running counts of annual MCS event days show general agreement between OBS and CTRL from

January until August (Figure 1a). QLCS event day counts begin to diverge sooner (Figure 1b), and results in 29 fewer QLCS event days by September 1, with most of that difference occurring within the June–August period (24 QLCS event days per year). When examining non-QLCS event days, CTRL exhibits a general positive bias compared to

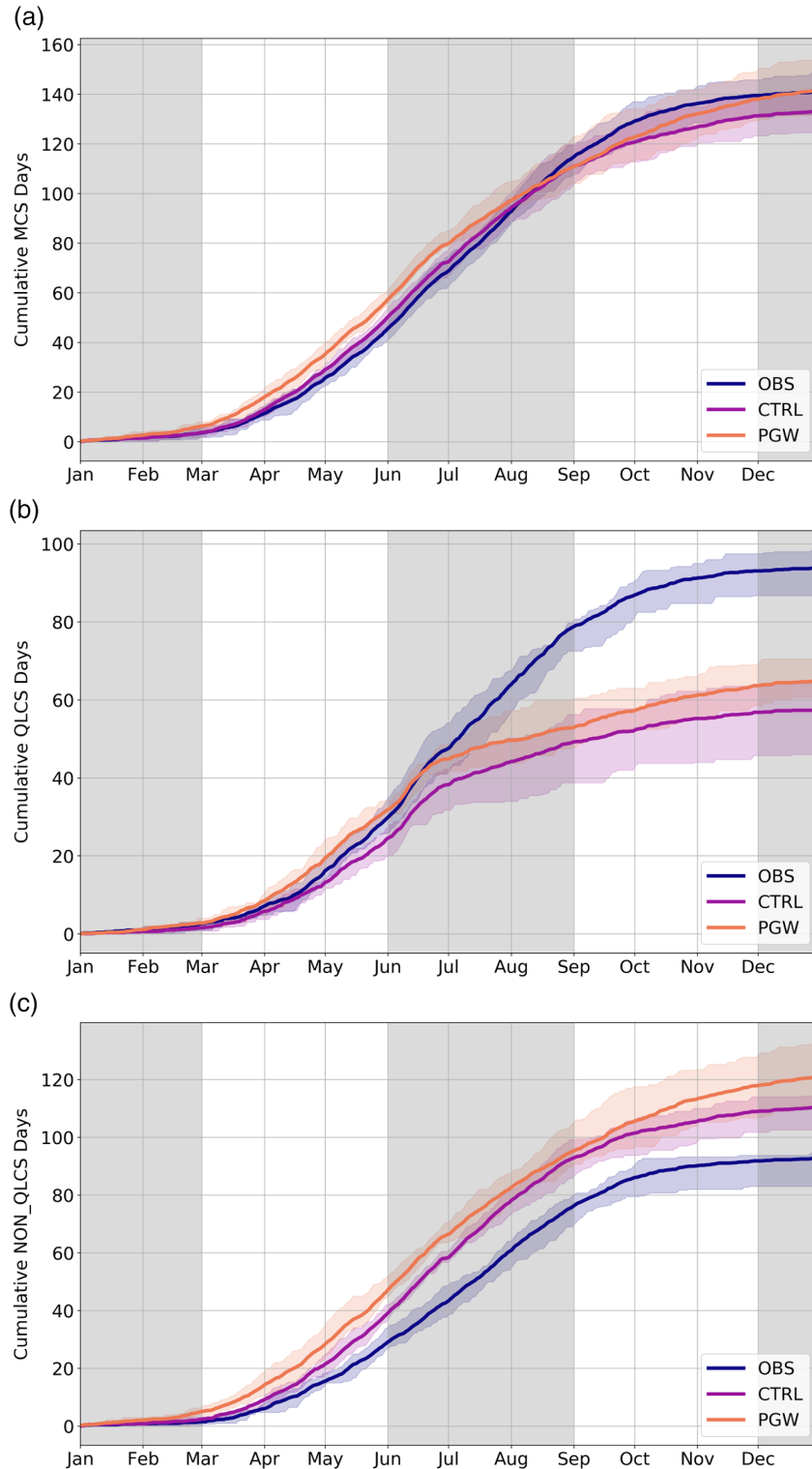


FIGURE 1 Mean counts of days (1800 UTC to 1800 UTC) that experienced at least one MCS or MCS subtype (2001–2012) in the Midwest CONUS for: (a) MCS, (b) QLCS, and (c) non-QLCS for the OBS, CTRL, and PGW runs. The filled regions represent the interquartile range over the 12-year period for cumulative swath count totals on each day of the year. Years 2000 and 2013 were not included because the entire year is not available for the CTRL and PGW datasets [Colour figure can be viewed at wileyonlinelibrary.com]

OBS (Figure 1c), with a mean of 17 more non-QLCS days by September 1. In contrast to QLCS event day counts, the mean count of non-QLCS event days differs by seven event days per June–August period for OBS and CTRL.

The diurnal cycle of MCSs, QLCSs, and non-QLCSs counts during June, July, and August in the Midwest exhibit a characteristic nocturnal maximum and midday minimum (Figure 2; Geerts *et al.*, 2017; Prein *et al.*, 2017a, 2017b). Of

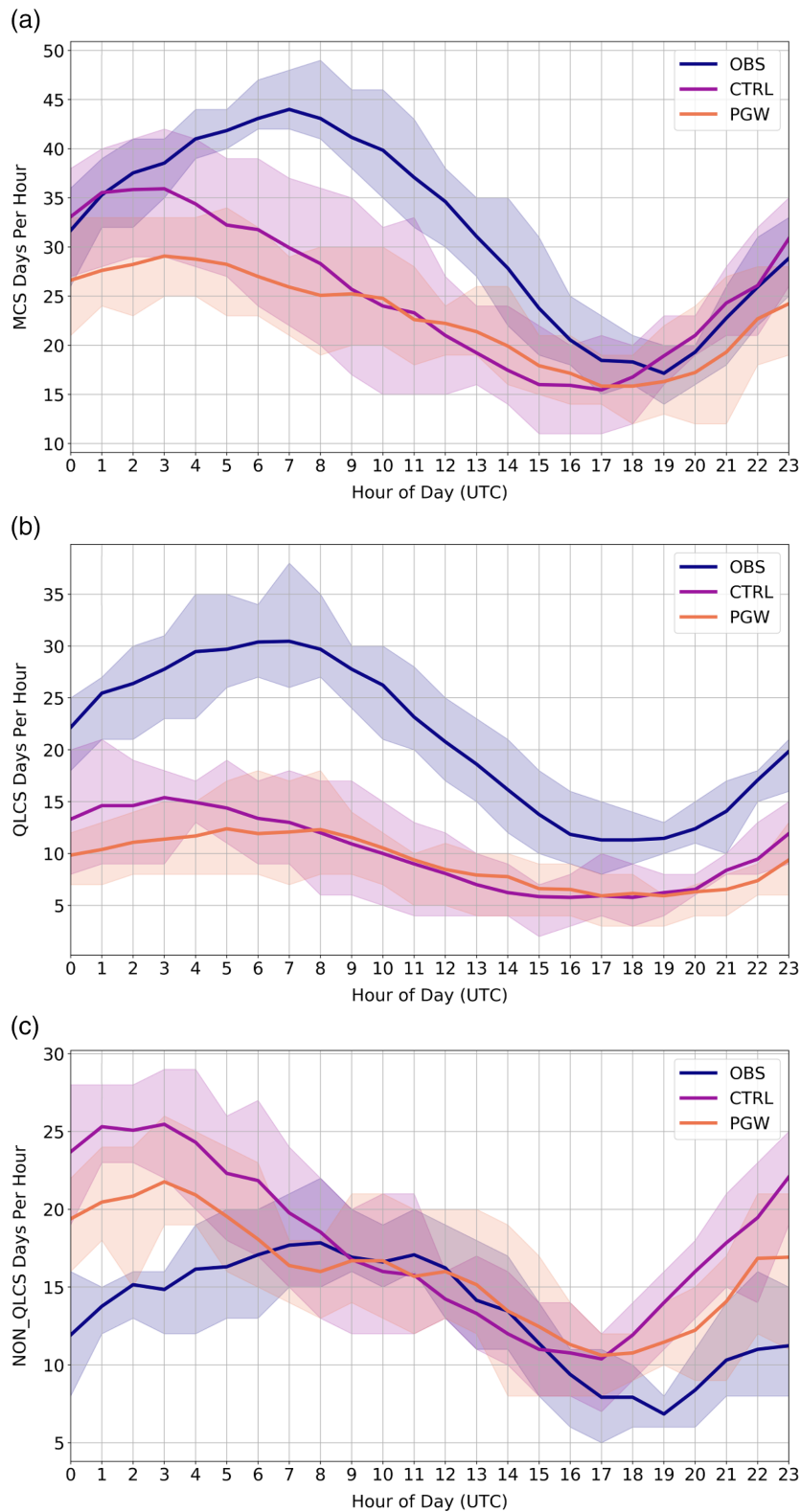


FIGURE 2 Counts of days where at least one of the following events occurred at a particular hour (UTC) during the summertime (2001–2013) in the Midwest CONUS: (a) MCS, (b) QLCS, and (c) non-QLCS for the OBS, CTRL, and PGW runs. The filled regions represent the interquartile range over the 13-year period for swath count totals for each hour of the day. Year 2000 was not included because summertime data are not available for the CTRL and PGW datasets [Colour figure can be viewed at wileyonlinelibrary.com]

the 1,196 available June, July, and August (JJA) days during the study period (2001–2013), mean OBS MCS event day frequency peaks at 0700 UTC (48%) and reaches a minimum at 1900 UTC (19%). OBS QLCS event day frequency peaks at 0600 UTC (33%), and minimizes at 1700 UTC (12%). Although OBS non-QLCS event days also peak overnight (0800 UTC) and reach a minimum in the middle of the day (1900 UTC), the maximum difference in the frequency of event day counts is only 12%, compared to 21% for QLCSs. For CTRL, MCS event day frequency peaks at 0300 UTC (39%), in comparison to CTRL QLCS and non-QLCS event day frequency, which also peaks at 0300 UTC (17 and 28%, respectively). Despite similar diurnal distributions of events, the absolute hourly event day counts between OBS and CTRL show some disparity, particularly during the evening and overnight hours (0000–1200 UTC). The maximum difference of roughly 15 fewer CTRL MCS event days per year occurs at 1000 UTC, with the minimum difference occurring at 2200 UTC (less than 1 fewer OBS MCS event days/year). For QLCSs, the disparity peaks at 0800 UTC with a difference of roughly 18 fewer CTRL QLCS event days per year, and minimum difference at 1900 UTC (5 fewer CTRL QLCS days per year). For non-QLCS, the maximum difference occurs at 0000 UTC, with CTRL producing roughly 12 more non-QLCS event days compared to OBS. The minimum difference occurs at 0900 UTC, where the mean count of non-QLCS event days per year differs by less than 1.

These disparities prompted further examination of the spatial structure of the data. Since MCS activity peaks in the summer, and the largest biases were found during this period, the spatial analysis will focus on the June–August period (Figure 3). QLCS counts for both CTRL (Figure 3a) and OBS (Figure 3b) show a relative peak in activity in the Midwest CONUS that extends to the Southern Plains. Despite this, the absolute counts for OBS QLCSs event days are much higher than CTRL QLCS event days, with a maximum difference over eastern Iowa of 91 QLCS event days (7 QLCSs event days per year). OBS non-QLCS counts (Figure 3d) are greater than CTRL non-QLCS (Figure 3c) counts in the Southern Plains and Southern Mississippi River Valley (up to 2 more non-QLCS days per year). CTRL non-QLCS counts are greater than OBS non-QLCS counts elsewhere, especially south and east of the Appalachians (up to 6 more non-QLCS days per year) and in the northwest Midwest (up to 4 more non-QLCS days per year). In general, the proportion of MCS events that are QLCSs in CTRL (Figure 3e) is much lower compared to OBS (Figure 3f). For all grids in the Midwest, the majority of OBS MCS days experience at least one QLCS. This proportion maximizes in Illinois, Iowa, Wisconsin, Missouri and Michigan where over 70% of MCS days experience a QLCSs (the opposite pattern exists for non-QLCSs). In contrast, the maximum proportion of CTRL MCS events that are QLCSs occurs in

central Texas, and many locations in the Midwest have proportions below 50%. In both CTRL and OBS, the ratio of QLCS to non-QLCS events is much lower in the Southeast CONUS compared to the Midwest.

To test if these spatial differences are significant, yearly distributions of counts are compared between OBS and CTRL for each grid cell using a Kolmogorov - Smirnov (KS) test (Wilks, 2006). p -Value significance thresholds are determined using the false discovery rate (FDR) method with an α_{FDR} of 0.10 (Wilks, 2016) to account for issues related to multiple hypothesis tests. For many locations in the Midwest, CTRL QLCS counts are underestimated by 70–85% compared to OBS, and these differences are significant, particularly in the southeastern portion of the study area (Figure 4). In contrast, CTRL non-QLCS events exhibit fewer significant differences in the southeast portion of the Midwest, whereas the differences are largely significant in the northwest portion of the Midwest. When comparing CTRL and PGW (i.e., early vs. late-21st century event counts), the differences between the event day counts of QLCSs (Figure 4c) or non-QLCSs (Figure 4d) days exhibit no field significance.

4 | DISCUSSION

QLCS day counts in the Midwest are generally underestimated in CTRL compared to OBS, whereas non-QLCS day counts are generally overestimated in both datasets. However, the results suggest that the negative bias in summertime CTRL MCS events in the Midwest (Prein *et al.*, 2017a) is driven by the model generating too few QLCS event days. As a result, the June, July, and August negative precipitation bias in this region (Liu *et al.*, 2017), as well as disparities related to radar-derived reflectivity bins (Rasmussen *et al.*, 2017) are likely owed to this deficiency. Prein *et al.* (2017a) offer a number of reasons for these biases related to CTRL MCSs, including: (a) failed upstream MCS initiation, (b) weaker large-scale forcing, (c) poor representation of soil–atmosphere interactions, and (d) a summertime dry bias. The attribution of these biases to poor QLCS representation may offer additional insight into this issue. QLCSs (bow echoes, leading line trailing stratiform, line echo wave patterns, etc.) are not represented well in numerical simulations compared to other MCS subtypes (Adams-Selin *et al.*, 2013; Snively and Gallus, 2014; Lawson and Gallus, 2016), and their accurate representation in RCMs is an area of ongoing research. For example, Lawson and Gallus (2016) found that WRF runs failed to produce bow echoes in the majority of sensitivity tests, despite using many different microphysics schemes and initial and lateral boundary condition perturbations. These events typically begin as isolated convective cells that grow upscale and form surface cold pools (Corfidi, 2003; Keene and Schumacher, 2013). New

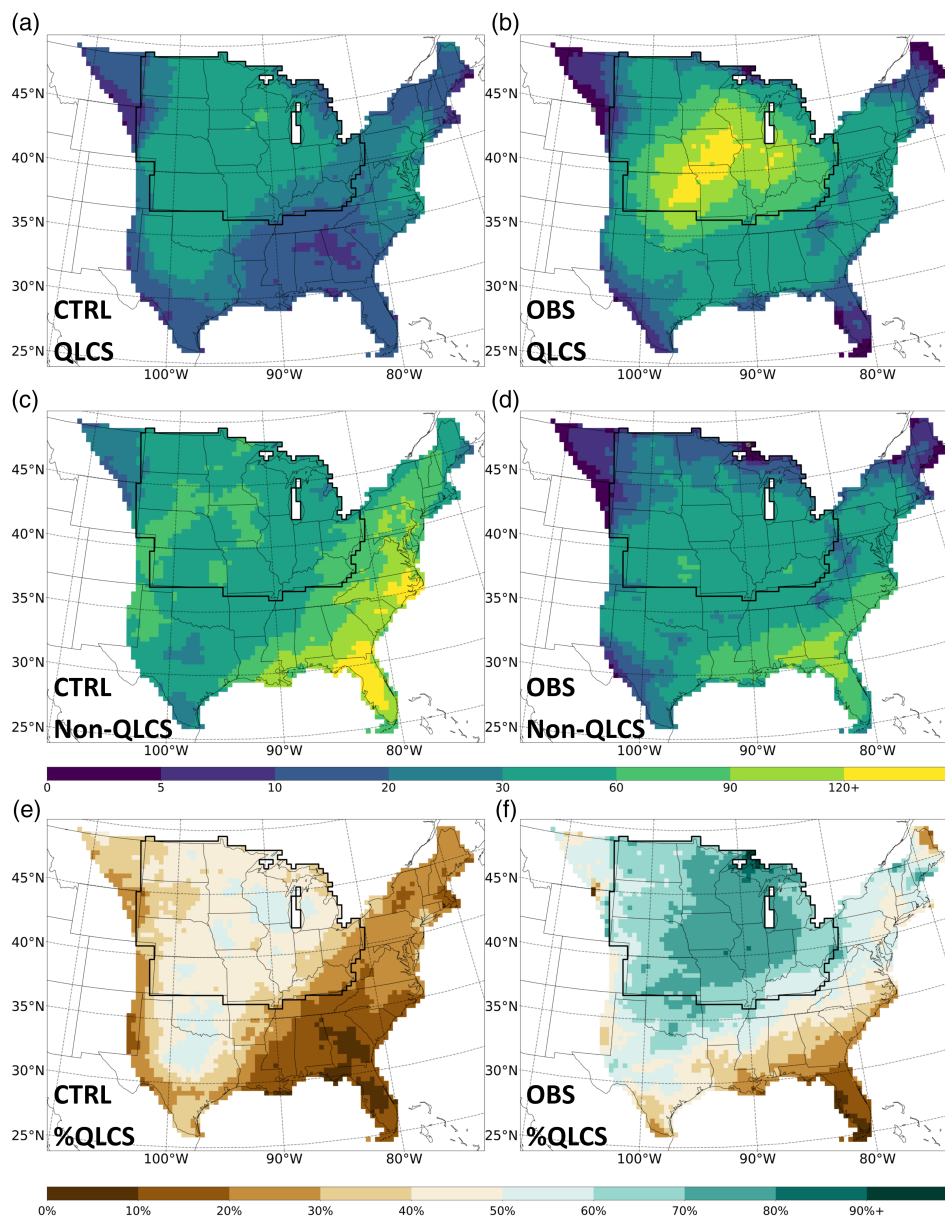


FIGURE 3 Summertime (June–August) spatial occurrence (mean per 40×40 km grid; 2001–2013) of days (1800 UTC–1800 UTC) that experienced at least one (a) CTRL QLCS, (b) OBS QLCS, (c) CTRL non-QLCS, and (d) OBS non-QLCS. In addition, the percentage of total MCS days that experienced at least one MCS subtype is illustrated for (e) CTRL and (f) OBS. The Midwest CONUS, as defined by this study, is delineated by a black outline [Colour figure can be viewed at wileyonlinelibrary.com]

convective cells form on the leading edge of the cold pool, effectively sustaining the system through reinforcing, complementary, mechanisms in supportive atmospheric environments (Rotunno *et al.*, 1988; Coniglio *et al.*, 2012). This process can be inferred by a “bowing” line of convection in radar images (Corfidi, 2003; Lawson and Gallus, 2016). Poor representation of cool pools or their “in situ” forcing may cause a variety of issues, including decreased longevity and weaker convective updraughts (Rotunno *et al.*, 1988; Corfidi, 2003). In addition, composites of MCSs and their environments in multiyear climate simulations show that MCSs can significantly influence their large-scale environment (Yang *et al.*, 2017), which can result in longer lived events.

Since QLCSs make up the majority of summertime MCSs in the Midwest CONUS, it is crucial for these events to be accurately represented in climate simulations, as they are an important component of the hydroclimate over critical agricultural regions (Ashley *et al.*, 2003; Prein *et al.*, 2017a, 2017b). In addition, many QLCSs produce tornadoes, wind, hail, and/or flooding in the Midwest CONUS (Trapp *et al.*, 2005; Gallus *et al.*, 2008), and future severe weather occurrence may be misrepresented if QLCS structures are not accurately reproduced. Future work should: (a) examine additional long-term, convection-permitting, climate simulations to see if this issue is isolated or widespread; (b) examine the long-term behaviour of cold pools associated with summertime Midwest QLCS events; and

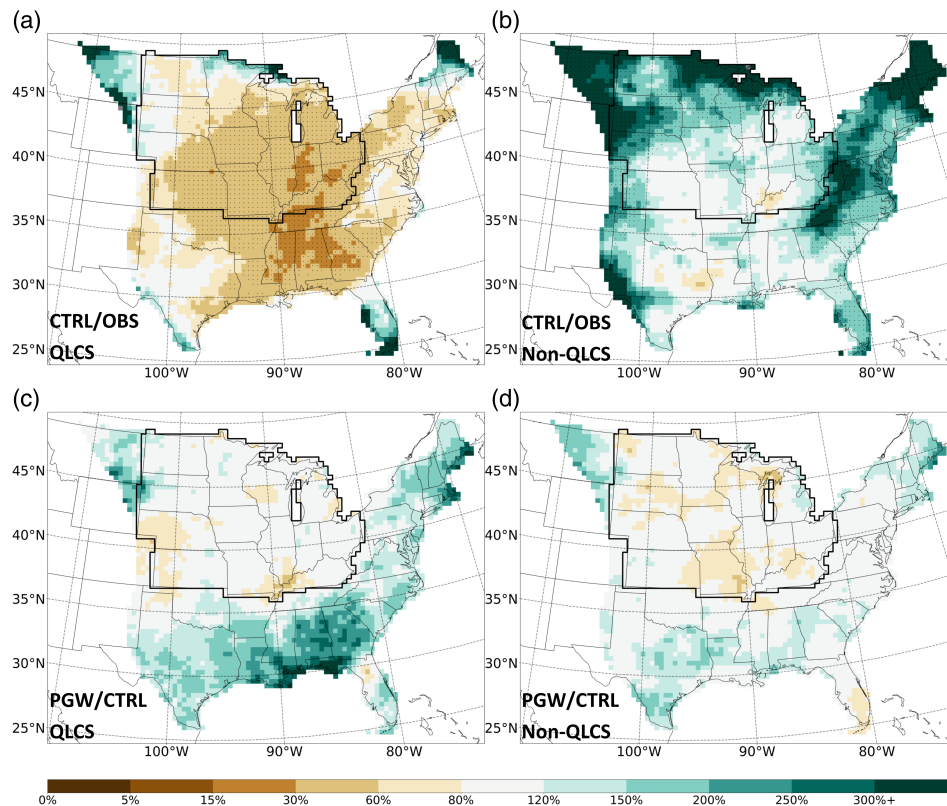


FIGURE 4 Summertime percent difference between the count of days where at least one MCS subtype event occurred for: (a, b) CTRL and OBS and (c, d) CTRL and PGW datasets for (a, c) Q LCSs and (b, d) non-Q LCSs. Percent difference is calculated by (a, b) dividing OBS grid cell values by corresponding CTRL grid cell values and (c, d) dividing CTRL grid cell values by corresponding PGW grid cell values. The stippling denotes significantly different distributions of yearly counts within all eastern CONUS grids using the FDR approach ($\alpha_{\text{FDR}} = 0.10$; Wilks, 2016) [Colour figure can be viewed at wileyonlinelibrary.com]

(c) explore the differences (if any) between how non-Q LCSs and Q LCSs modify the large-scale environment using synoptic-scale composites of events (e.g., Yang *et al.*, 2017).

ACKNOWLEDGEMENTS

The authors would like to thank Drs. Russ Schumacher (Colorado State University), Victor Gensini (NIU), David Changnon (NIU), Thomas Pingel (NIU), and Jie Zhou (NIU), for their suggestions and insight that improved the research and paper. The authors would also like to thank Drs. Kyoko Ikeda and Andreas Prein for their assistance in accessing and interpreting the climate simulation data; and Arthur Person (Senior Research Assistant at The Pennsylvania State University, Department of Meteorology) for providing computational resources. In addition, The authors would like to thank Dr. Ian McKendry and two anonymous reviewers for greatly improving this manuscript. This research was supported by National Science Foundation Grant ATM-1637225, an NIU Division of Research and Innovation Partnerships Research and Artistry Grant, and an NIU Graduate School Dissertation Completion Fellowship. This work used resources of the Center for Research Computing and Data at Northern Illinois University. The analysis data and code used for this article is available at [https://](https://github.com/ahaberlie/MCS/)

github.com/ahaberlie/MCS/. The convection-permitting climate simulation data used for this work are available online (<https://rda.ucar.edu/datasets/ds612.0/>).

ORCID

Alex M. Haberlie  <https://orcid.org/0000-0001-9172-4028>

Walker S. Ashley  <https://orcid.org/0000-0003-0816-3333>

REFERENCES

- Adams-Selin, R.D., van den Heever, S.C. and Johnson, R.H. (2013) Sensitivity of bow-echo simulation to microphysical parameterizations. *Weather and Forecasting*, 28, 1188–1209.
- Ashley, W.S., Mote, T.L., Dixon, P.G., Trotter, S.L., Powell, E.J., Durkee, J.D. and Grundstein, A.J. (2003) Distribution of mesoscale convective complex rainfall in the United States. *Monthly Weather Review*, 131, 3003–3017.
- Clark, A.J., Bullock, R.G., Jensen, T.L., Xue, M. and Kong, F. (2014) Application of object-based time-domain diagnostics for tracking precipitation systems in convection-allowing models. *Weather and Forecasting*, 29, 517–542.
- Coniglio, M.C., Corfidi, S.F. and Kain, J.S. (2012) Views on applying RKW theory: an illustration using the 8 May 2009 derecho-producing convective system. *Monthly Weather Review*, 140, 1023–1043.
- Corfidi, S.F. (2003) Cold pools and mcs propagation: forecasting the motion of downwind-developing mcs. *Weather and Forecasting*, 18, 997–1017.
- Dee, D.P., Uppala, S., Simmons, A., Berrisford, P., Poli, P., Kobayashi, S., et al. (2011) The era-interim reanalysis: configuration and performance of the data assimilation system. *Quarterly Journal of the Royal Meteorological Society*, 137, 553–597.

- Dieleman, S., Willett, K.W. and Dambre, J. (2015) Rotation-invariant convolutional neural networks for galaxy morphology prediction. *Monthly Notices of the Royal Astronomical Society*, 450, 1441–1459.
- Diffenbaugh, N.S., Trapp, R.J. and Brooks, H. (2008) Does global warming influence tornado activity? *Eos, Transactions, American Geophysical Union*, 89, 553–554.
- Fabry, F., Meunier, V., Treserras, B.P., Cournoyer, A. and Nelson, B. (2017) On the climatological use of radar data mosaics: possibilities and challenges. *The Bulletin of the American Meteorological Society*, 98, 2135–2148.
- Feng, Z., Leung, L.R., Hagos, S., Houze, R.A., Burleyson, C.D. and Balaguru, K. (2016) More frequent intense and long-lived storms dominate the springtime trend in central us rainfall. *Nature Communications*, 7, 13429.
- Gagne, D.J., Haupt, S.E. and Nychka, D.W. (2017) Evaluation of deep learning representations of spatial storm data. In: *AGU Fall Meeting Abstracts*. New Orleans, LA: American Geophysical Union.
- Gallus, W.A., Snook, N.A. and Johnson, E.V. (2008) Spring and summer severe weather reports over the Midwest as a function of convective mode: a preliminary study. *Weather and Forecasting*, 23, 101–113.
- Geerts, B., Parsons, D., Ziegler, C.L., Weckwerth, T.M., Biggerstaff, M.I., Clark, R.D., Coniglio, M.C., Demoz, B.B., Ferrare, R.A., Gallus, W.A., Jr., Haghi, K., Hanesiak, J.M., Klein, P.M., Knupp, K.R., Kosiba, K., McFarquhar, G.M., Moore, J.A., Nehrir, A.R., Parker, M.D., Pinto, J.O., Rauber, R.M., Schumacher, R.S., Turner, D.D., Wang, Q., Wang, X., Wang, Z. and Wurman, J. (2017) The 2015 plains elevated convection at night field project. *The Bulletin of the American Meteorological Society*, 98, 767–786.
- Gensini, V.A. and Mote, T.L. (2014) Estimations of hazardous convective weather in the United States using dynamical downscaling. *Journal of Climate*, 27, 6581–6589.
- Haberlie, A.M. and Ashley, W.S. (2018a) A method for identifying midlatitude mesoscale convective systems in radar mosaics. Part I: Segmentation and classification. *Journal of Applied Meteorology and Climatology*, 57, 1575–1598.
- Haberlie, A.M. and Ashley, W.S. (2018b) A method for identifying midlatitude mesoscale convective systems in radar mosaics. Part II: Tracking. *Journal of Applied Meteorology and Climatology*, 57, 1599–1621.
- Harding, K.J. and Snyder, P.K. (2015) Using dynamical downscaling to examine mechanisms contributing to the intensification of central us heavy rainfall events. *Journal of Geophysical Research – Atmospheres*, 120, 2754–2772.
- Herman, G.R. and Schumacher, R.S. (2016) Extreme precipitation in models: an evaluation. *Weather and Forecasting*, 31, 1853–1879.
- Houze, R.A. (2004) Mesoscale convective systems. *Reviews of Geophysics*, 42, 1–43.
- Ikeda, K., Rasmussen, R., Liu, C., Gochis, D., Yates, D., Chen, F., Tewari, M., Barlage, M., Dudhia, J., Miller, K., Arsenault, K., Grubišić, V., Thompson, G. and Guttman, E. (2010) Simulation of seasonal snowfall over Colorado. *Atmospheric Research*, 97, 462–477.
- IPCC. (2013) *Climate Change 2013: The Physical Science Basis. Contribution of Working Group I to the Fifth Assessment Report of the Intergovernmental Panel on Climate Change*. Cambridge, UK and New York, NY: Cambridge University Press, p. 1535.
- Keene, K.M. and Schumacher, R.S. (2013) The bow and arrow mesoscale convective structure. *Monthly Weather Review*, 141, 1648–1672.
- Kendon, E.J., Roberts, N.M., Fowler, H.J., Roberts, M.J., Chan, S.C. and Senior, C.A. (2014) Heavier summer downpours with climate change revealed by weather forecast resolution model. *Nature Climate Change*, 4, 570–576.
- Krizhevsky, A., Sutskever, I. and Hinton, G.E. (2012) Imagenet classification with deep convolutional neural networks. In: *Advances in Neural Information Processing Systems*. Lake Tahoe, NV: Neural Information Processing Systems Conference and Workshop, pp. 1097–1105.
- Kunkel, K.E., Karl, T.R., Brooks, H., Kossin, J., Lawrimore, J.H., Arndt, D., Bosart, L., Changnon D., Cutter, S.L., Doesken, N., Emanuel, K., Groisman P.Y., Katz, R.W., Knutson, T., O'Brien, J., Paciorek, C.J., Peterson, T.C., Redmond, K., Robinson, D., Trapp, J., Vose, R., Weaver, S., Wehner, M., Wolter, K. and Wuebbles, D. (2013) Monitoring and understanding trends in extreme storms: state of knowledge. *The Bulletin of the American Meteorological Society*, 94, 499–514.
- Lakshmanan, V., Miller, M. and Smith, T. (2013) Quality control of accumulated fields by applying spatial and temporal constraints. *Journal of Atmospheric and Oceanic Technology*, 30, 745–758.
- Lawson, J. and Gallus, W.A. (2016) On contrasting ensemble simulations of two great plains bow echoes. *Weather and Forecasting*, 31, 787–810.
- Liu, C., Ikeda, K., Rasmussen, R., Barlage, M., Newman, A.J., Prein, A.F., Chen, F., Chen, L., Clark, M., Dai, A., Dudhia, J., Eidhammer, T., Gochis, D., Gutmann, E., Kurkute, S., Li, Y., Thompson, G. and Yates, D. (2017) Continental-scale convection-permitting modeling of the current and future climate of north america. *Climate Dynamics*, 49, 71–95.
- Matyas, C.J. (2010) Use of ground-based radar for climate-scale studies of weather and rainfall. *Geography Compass*, 4, 1218–1237.
- Matyas, C.J., Zick, S.E. and Tang, J. (2018) Using an object-based approach to quantify the spatial structure of reflectivity regions in hurricane Isabel (2003). Part I: comparisons between radar observations and model simulations. *Monthly Weather Review*, 146, 1319–1340.
- McGovern, A., Elmore, K.L., Gagne, D.J., Haupt, S.E., Karstens, C.D., Lagerquist, R., Smith, T. and Williams, J.K. (2017) Using artificial intelligence to improve real-time decision-making for high-impact weather. *The Bulletin of the American Meteorological Society*, 98, 2073–2090.
- Munkres, J. (1957) Algorithms for the assignment and transportation problems. *SIAM Journal on Applied Mathematics*, 5, 32–38.
- Novak, D.R., Bailey, C., Brill, K.F., Burke, P., Hogsett, W.A., Rausch, R. and Schichtel, M. (2014) Precipitation and temperature forecast performance at the weather prediction center. *Weather and Forecasting*, 29, 489–504.
- Parker, M.D. and Johnson, R.H. (2000) Organizational modes of midlatitude mesoscale convective systems. *Monthly Weather Review*, 128, 3413–3436.
- Prein, A.F., Langhans, W., Fossier, G., Ferrone, A., Ban, N., Goergen, K., Keller, M., Tolle, M., Gutjahr, O., Feser, F., Brisson, E., Kollet, S., Schmidli, J., van Lipzig, N.P.M. and Leung, R. (2015) A review on regional convection-permitting climate modeling: demonstrations, prospects, and challenges. *Reviews of Geophysics*, 53, 323–361.
- Prein, A.F., Liu, C., Ikeda, K., Bullock, R., Rasmussen, R.M., Holland, G.J. and Clark, M. (2017a) Simulating north American mesoscale convective systems with a convection-permitting climate model. *Climate Dynamics*, 1–16. <https://doi.org/10.1007/s00382-017-3993-2>
- Prein, A.F., Liu, C., Ikeda, K., Trier, S.B., Rasmussen, R.M., Holland, G.J. and Clark, M.P. (2017b) Increased rainfall volume from future convective storms in the us. *Nature Climate Change*, 7, 880.
- Rasmussen, K., Prein, A., Rasmussen, R., Ikeda, K. and Liu, C. (2017) Changes in the convective population and thermodynamic environments in convection-permitting regional climate simulations over the United States. *Climate Dynamics*, 1–26. <https://doi.org/10.1007/s00382-017-4000-7>
- Rotunno, R., Klemp, J.B. and Weisman, M.L. (1988) A theory for strong, long-lived squall lines. *Journal of the Atmospheric Sciences*, 45, 463–485.
- Smith, A.B. and Katz, R.W. (2013) Us billion-dollar weather and climate disasters: data sources, trends, accuracy and biases. *Natural Hazards*, 67, 387–410.
- Snively, D.V. and Gallus, W.A. (2014) Prediction of convective morphology in near-cloud-permitting wrf model simulations. *Weather and Forecasting*, 29, 130–149.
- Stevenson, S.N. and Schumacher, R.S. (2014) A 10-year survey of extreme rainfall events in the central and eastern United States using gridded multisensor precipitation analyses. *Monthly Weather Review*, 142, 3147–3162.
- Tang, Y., Winkler, J., Zhong, S., Bian, X., Doubler, D., Yu, L. and Walters, C. (2017) Future changes in the climatology of the great plains low-level jet derived from fine resolution multi-model simulations. *Scientific Reports*, 7, 5029.
- Tippett, M.K., Allen, J.T., Gensini, V.A. and Brooks, H.E. (2015) Climate and hazardous convective weather. *Current Climate Change Reports*, 1, 60–73.
- Trapp, R.J., Tessendorf, S.A., Godfrey, E.S. and Brooks, H.E. (2005) Tornadoes from squall lines and bow echoes. Part I: climatological distribution. *Weather and Forecasting*, 20, 23–34.
- Trapp, R.J., Robinson, E.D., Baldwin, M.E., Diffenbaugh, N.S. and Schwedler, B. R. (2011) Regional climate of hazardous convective weather through high-resolution dynamical downscaling. *Climate Dynamics*, 37, 677–688.
- Weisman, M.L., Skamarock, W.C. and Klemp, J.B. (1997) The resolution dependence of explicitly modeled convective systems. *Monthly Weather Review*, 125, 527–548.
- Wilks, D.S. (2006) *Statistical Methods in the Atmospheric Sciences. International Geophysics Series*, Vol. 91, 2nd edition. Burlington, MA: Academic Press, p. 627.
- Wilks, D.S. (2016) “The stippling shows statistically significant grid points”: how research results are routinely overstated and overinterpreted, and what to do about it. *The Bulletin of the American Meteorological Society*, 97, 2263–2273.

Yang, Q., Houze, R.A., Leung, L.R. and Feng, Z. (2017) Environments of long-lived mesoscale convective systems over the Central United States in convection permitting climate simulations. *Journal of Geophysical Research – Atmospheres*, 122, 13288–13307.

SUPPORTING INFORMATION

Additional supporting information may be found online in the Supporting Information section at the end of the article.

How to cite this article: Haberlie AM, Ashley WS. Climatological representation of mesoscale convective systems in a dynamically downscaled climate simulation. *Int J Climatol.* 2018;1–10. <https://doi.org/10.1002/joc.5880>